Available online at www.sciencedirect.com
SCIENCE DIRECT®
ELSEVIER
Nuclear Instruments and Methods in Physics Research B 202 (2003) 188–194
NIM B
Beam Interactions with Materials & Atoms
www.elsevier.com/locate/nimb

Photochemical ablation of organic solids

Yaroslava G. Yingling, Barbara J. Garrison *

Department of Chemistry, 152 Davey Laboratory, The Pennsylvania State University, University Park, PA 16802, USA

Abstract

We have investigated by molecular dynamics simulations the ablation of material that is onset by photochemical processes. We compare this system with only photochemical processes to a system containing photochemical and photothermal processes. The simulations reveal that ablation by purely photochemical processes is accompanied by the ejection of relatively cold massive molecular clusters from the surface of the sample. The top of the plume exhibits high temperatures whereas the residual part of the sample is cold. The removal of the damaged material through big molecular cluster ejection is consistent with experimental observations of low heat damage of material.

PACS: 61.80.Az; 02.70.Ns
Keywords: Molecular dynamics simulations; Laser ablation; Photochemical fragmentation; Photochemical processes

1. Introduction

There are two dominant processes responsible for the onset of ablation – photochemical processes that break chemical bonds in the molecule and photothermal processes that heat the sample. It is generally believed for lasers operating at visible or infrared wavelengths, that photothermal processes in the sample are dominant. With the far-UV (<200 nm) laser irradiation, when the photon energy is larger than the energy of the chemical bonds in the molecule, photochemical processes are responsible for the onset of ablation. Since the photothermal and photochemical processes are coupled with each other in UV ablation, the question of the relative importance of these two processes in ablation mechanism is raised [1–4].

Evidence of photochemical processes in laser ablation can be associated with the composition change with respect to IR ablation of similar samples; no significant heat damage of the remaining material; high ablation rates; large number of various species with high translational energies; non-equilibrium between the translational, vibrational, and rotational temperatures of ablated products; presence of shock wave propagation with high initial velocity; high gas-like plume density; fast surface swelling; and low threshold value [2,5–11]. Due to complexity of the processes involved, the understanding of the role of photochemical processes in laser ablation remains a challenge.

Our group has developed a versatile mesoscopic molecular dynamics model for the investigation of laser ablation [12–19]. This model allows us to investigate both photochemical and/or photothermal

* Corresponding author. Tel.: +1-814-863-2103; fax: +1-814-863-5319.
E-mail address: bjg@psu.edu (B.J. Garrison).

0168-583X/02/$ - see front matter
doi:10.1016/S0168-583X(02)01855-4

processes in detail. In our previous publications, the combination of photothermal and photochemical processes in UV ablation on the material removal mechanism has been examined [17,18,20]. It has been reported that the presence of photochemical processes has lowered the ablation threshold due to the release of additional energy from exothermic reactions into the irradiated sample and due to the decrease of the average attractive bonding in the absorbing region [17]. In addition, the photochemical fragmentation and the consequent chemical reactions have created an additional local pressure build up and have generated a strong acoustic pressure wave propagation toward the bottom of the computational cell. This strong pressure wave and increase of the temperature in the absorbing region were responsible for the ejection of big molecular clusters resulting in high molecular yields. The ejected clusters disintegrate into smaller clusters and monomers after the laser pulse due to ongoing chemical reactions in the plume. The ejection and disintegration of big clusters result in the high material removal rates and high plume density [20]. The results from our computational study have shown a good agreement with experimental observations, in which the higher ablation rates, low threshold, strong pressure wave propagation, and high plume density were attributed to the presence of photochemistry [6–8].

In order to investigate pure photoablation of organic solids, a simulation containing only photochemical excitations has been performed. In this publication, the results of this pure photochemical system are compared to the results from the system containing both photochemical and thermal processes. The differences in temporal enthalpy profiles, pressure wave propagation and densities of the plume are discussed. Our simulations provide a unique perspective on the laser ablation phenomena at the molecular level and provide microscopic insights into the experimental investigations of laser ablation.

2. Computational model

We have developed and applied a molecular dynamics model to investigate the role of the photochemical process in laser ablation in detail [17,18,20]. The complete description of the model is presented elsewhere [17]. The essential feature of this model is that each molecule is represented by a spherical particle that has true translational degrees of freedom but an approximate internal degree of freedom, i.e. the breathing mode [12–14]. The internal breathing mode allows one to control the rate of energy transfer from the excited molecule to the remaining solid. The absorption of a UV photon by the organic molecule can induce either vibrational excitation or photochemical fragmentation of the molecule. The vibrational excitation is modeled by depositing the photon energy into the kinetic energy of internal vibrations of the excited molecule. The photochemical decomposition of the excited molecule is represented by the rupture of the chemical bond inside the molecule, resulting in the formation of radicals. These radicals can subsequently undergo various abstraction and recombination reactions. The photofragmentation of the excited molecule and subsequent chemical reactions in our model are based on photochemistry of chlorobenzene. Photofragmentation of chlorobenzene occurs via scission of the C–Cl bond to yield C_6H_5 and Cl radicals, which in solution and static gas cell experiments react with each other and the parent molecule to form a number of different products, such as HCl, Cl_2, C_6H_6, $C_6H_4Cl_2$, $C_{12}H_{10}$, $C_{12}H_9Cl$ and $C_{12}H_8Cl_2$ [3,4,21].

In our model, we include the chemical reactions that are thermodynamically favorable and are observed in gas-phase or solution chemistry of chlorobenzene. Each photoproduct or photofragment is represented as a spherical particle with an individual set of interaction potential parameters, mass and size. For each reaction the standard heat of formation, $\Delta H^0_{\mathrm{rxn}}$, is calculated from the available thermochemical data. When any of these reactions occur, the corresponding $\Delta H^0_{\mathrm{rxn}}$ will be the change in the total (potential plus kinetic) energy of the reactions products and surrounding molecules. The amount of energy given off from each reaction depends on the phase of the surroundings and is carefully monitored by adjusting initial positions of the reaction products and by performing additional local energy checks.

The complete list of the reactions induced by the laser excitation and subsequent photodecomposition of chlorobenzene, which are included in the model, is presented in [17]. Below are some examples of the simulated reactions.

Laser excitation of the molecule:

$$C_6H_5Cl + h\nu \rightarrow C_6H_5Cl^*.$$

Photochemical fragmentation of the excited molecule:

$$C_6H_5Cl^* \rightarrow C_6H_5^{\cdot} + {}^{\cdot}Cl,$$
$$\Delta H^0_{rxn} = -79.5 \text{ kJ/mol}.$$

Vibrational relaxation of the excited molecule:

$$C_6H_5Cl^* \rightarrow C_6H_5Cl, \quad \Delta H^0_{rxn} = -482.7 \text{ kJ/mol}.$$

Abstraction reaction:

$$C_6H_5Cl + {}^{\cdot}Cl \rightarrow C_6H_4Cl^{\cdot} + HCl,$$
$$\Delta H^0_{rxn} = \text{from} - 109.3 \text{ to} - 66.4 \text{ kJ/mol}.$$

Radical–radical recombination reactions:

$$C_6H_4Cl^{\cdot} + {}^{\cdot}C_6H_4Cl \rightarrow C_{12}H_8Cl_2,$$
$$\Delta H^0_{rxn} = \text{from} - 282.3 \text{ to} - 194.0 \text{ kJ/mol}.$$

$$C_6H_4Cl^{\cdot} + {}^{\cdot}C_6H_5 \rightarrow C_{12}H_9Cl,$$
$$\Delta H^0_{rxn} = -410.9 \text{ kJ/mol}.$$

The choice of the dynamics and probabilities of the reactions is explained in [17]. Briefly, the reaction probability depends on the distance between the reactant and the phase of surroundings. Many energetic reactions occur in the liquid or gas phase only. Generally, recombination reactions are faster than abstraction reactions. Hence, in the model two neighboring radicals react instantly with each other. However, the neighboring radical and the molecule can react only after the certain time, which depends on the lifetime and reactivity of the particular radical.

The simulations are performed on a computational cell with dimensions of $10 \times 10 \times 191$ nm (130,000 molecules). Periodic boundary conditions are imposed in the directions parallel to the surface. At the bottom of the sample, non-reflecting dynamic boundary conditions are applied [22]. The 248-nm laser irradiation is simulated by photochemical or vibrational excitation of randomly chosen molecules during the laser pulse of 150 ps within the penetration depth of 50 nm. The total number of photons entering the model during the laser pulse is controlled by the laser fluence. The exponential attenuation of the laser light with depth is modulated by the Lambert–Beer's law. The relative fraction of excited molecules that undergo photodecomposition can be set to the desired number. Although purely photochemical processes would be expected to only occur for wavelengths less than ~200 nm, we have used the 248 nm wavelength as the algorithms for specific chemical reactions, their exothermicities, and molecule placements have been established previously. To switch wavelengths is not trivial and would not aid in our understanding of the processes involved.

In order to use a relatively large system, a multiple step integration algorithm has to be employed. The time step of 5 fs is used in the parts of the system where no reactions occur or no free radicals are present. In the regions where reactions are taking place, the time step is decreased to 0.5 fs.

3. Results and discussion

We compare the results for the pure photochemical system to the system containing both photochemical and thermal processes. Specifically, this second system has 36% of excited molecules photofragmented and the rest are vibrationally excited. This specific percentage has been observed experimentally for 248-nm irradiation of a molecular beam of chlorobenzene [3]. For simplicity, the system containing both photochemical and thermal processes will be called a "combined" system throughout the remaining text of this publication.

In our previous study, we noticed that the increase of the photolysis rate decreases the ablation threshold fluence [17]. As expected the system where all excited molecules undergo photochemical fragmentation exhibits a lower threshold with respect to the combined system. For comparison,

we have chosen two simulations in which the total enthalpy released into the solid is approximately the same.

For these two systems, the enthalpy change per unit time is plotted versus time in Fig. 1. In the combined system, the enthalpy in the sample is defined by the photon energy and the number and nature of the photochemical reactions. In the pure photochemical system, the enthalpy change is determined only by the photochemical reactions. In the event of vibrational excitation, each photon absorbed increases the total enthalpy by 482.7 kJ/mol. All of this energy is available for translational motions of the molecules as well as internal energy in the breathing mode. In the event of photochemical fragmentation, the photon energy is mainly spent on the rupture of chemical bond inside the excited molecule, therefore, the enthalpy increases by a much smaller value of 80 kJ/mol. However, the subsequent exothermic chemical reactions increase the enthalpy by 30–500 kJ/mol per reaction. The enthalpy of reaction can be converted into the thermal energy of surroundings if the reaction is taking place in the solid, or into the translational energy of ablation if the reaction is taking place in the plume or top layers of the sample. The probability of reaction depends the phase of surroundings and the distance between the reactants, which is limited by diffusion and concentration of radicals. Indeed, the radicals begin to react when the top layers of the sample are melted and there is significant accumulation of the radicals inside the irradiated area. In the combined system, the enthalpy and the temperature increase faster than in pure photochemical system due to vibrational excitation of molecules. As a result, the reactions are starting to occur in the absorbing region after a few ps of laser pulse. In contrast, in the pure photochemical system, for the first 50 ps of laser pulse the enthalpy and the temperature of the sample increase slowly preventing formed radicals from undergoing reactions. By 50 ps, many radicals are formed in the absorbing area and are ready to react. Consequently, when the top layers melt, many chemical reactions take place in the top melted layers causing a sharp enthalpy increase. After the laser pulse is over, no more photofragmentation reactions take place, but the existing radicals continue to react and the rate of energy deposition decreases gradually. At the bottom of the absorbing region, the concentration of radicals is lower due to the exponential attenuation of laser light and the system is colder than in the combined system due to fragmentation of excited molecules. Therefore, chemical reactions are prevented. As a result, in the pure photochemical system, the top of the plume is hotter but the leftover sample is colder that in the combined system.

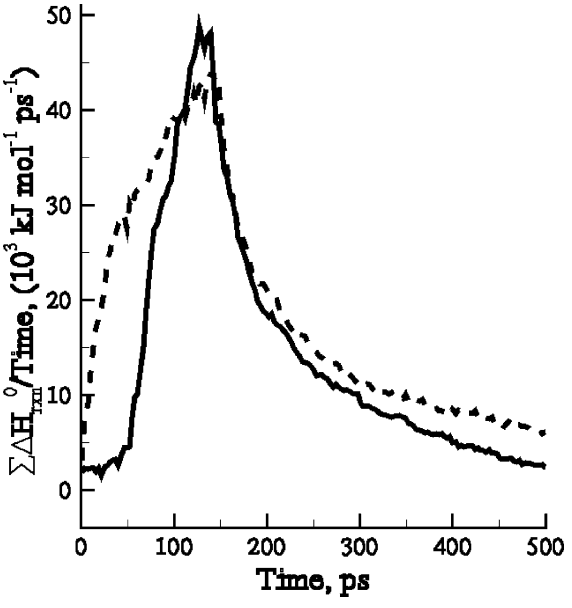

Fig. 1. The rate of enthalpy change in the sample versus time. The solid line represents the system with only photochemical excitation. The dashed line represents the system with photochemical and vibrational excitation.

The difference in the enthalpy profiles should be reflected in the acoustic pressure wave profiles propagating toward the bottom of the computational cell. The pressure dependence on time is plotted in Fig. 2 for the combined and the pure photochemical systems. The temporal pressure wave profiles are calculated at 100 nm below the surface. During the laser pulse the local pressure from reactions and/or vibrationally excited molecules builds up inside the absorbing region. Positive pressure is related to compressive stress. The

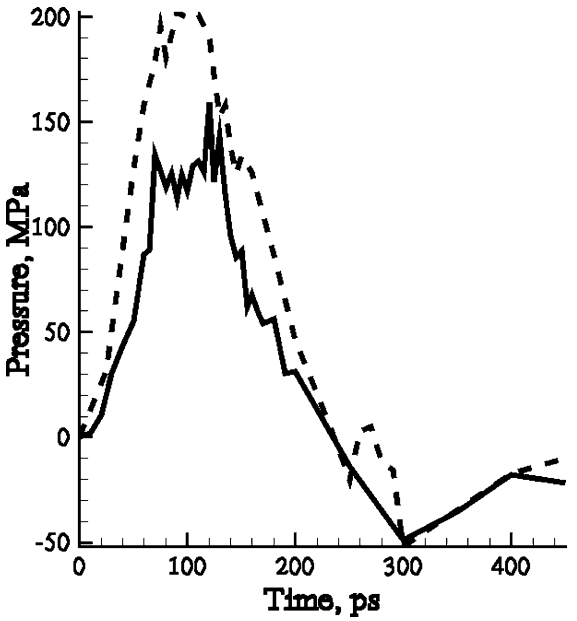

Fig. 2. Temporal pressure profiles at 100 nm below the surface. The solid line represents the system with only photochemical excitation. The dashed line represents the system with photochemical and vibrational excitation.

interaction of this pressure with the material leads to the development of the negative or tensile pressure. In a previous publication, we reported the development of strong and broad pressure wave in the combined system [20]. By looking at the temporal enthalpy profile (Fig. 1) one would expect the pressure wave for the pure photochemical system to be stronger but narrower than the pressure wave in combined system. The pressure wave in the pure photochemical system is not as broad but is less intense. The decrease in intensity is attributed to the occurrence of the highly exothermic reactions already in the plume, since by 150 ps the plume is already developed.

The strong pressure can cause spallation of the sample at the certain depth where tensile stresses exceed the dynamic tensile stress of the material [12,23]. The tensile strength of materials decreases significantly when the temperature increases. The pressure wave is stronger and the temperature of the sample is higher in the combined system, which results in the spallation of material deeper than in the pure photochemical system. As a result of this spallation, big chunks of material are removed from the surface into the plume for both simulations. This results in the higher yield in the combined system by approximately 19,000 molecules (30 nm) than the yield in the pure photochemical system.

The effects discussed above can be illustrated in Fig. 3 where the density profiles and corresponding snapshots near the surface of the irradiated sample are present for both simulations. At 100 ps, the system with pure photochemistry exhibits less thermal expansion than the combined system, which agrees with the information received from enthalpy profiles on Fig. 1. By 250 ps, the plume in

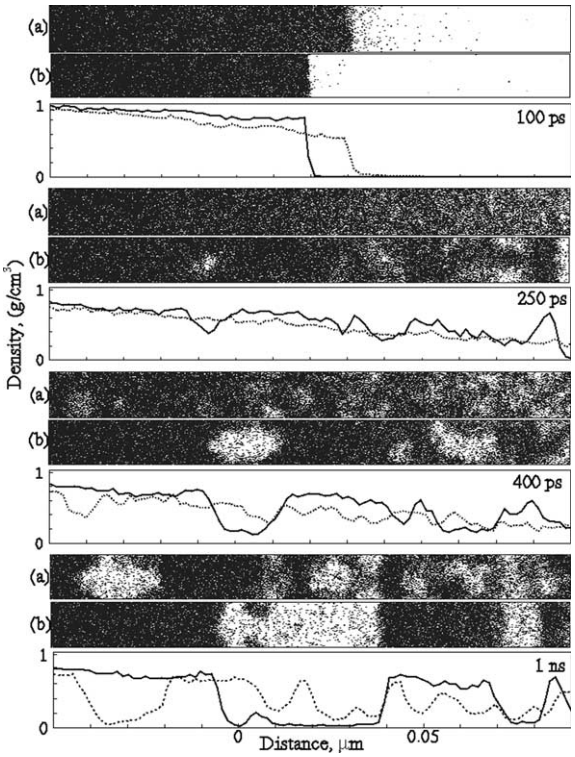

Fig. 3. Density profiles and corresponding snapshots near the surface of irradiated sample for (a) simulation with photochemical and vibrational excitations (dashed lines) and for (b) simulation with photochemical excitation only (solid lines). Data for four different times are given. The laser irradiates the sample from the right. The density of the original sample is 1.1064 g/cm^3. Distance 0 denotes the original surface.

both systems is fully developed. In the combined system, the density of the plume decreases monotonically with the distance from the original surface. In contrast, in the pure photochemical system, low and high density regions occur in the plume, indicating the formation of clusters. The low density regions are formed due to very fast increase in enthalpy (Fig. 1) and pressure wave propagation (Fig. 2) resulting in the spallation of the sample at 10 nm. The rupture of the sample at this depth can be attributed to the strong pressure gradient rather than to the occurrence of chemical reactions, resulting in the removal of the relatively cold and dense chunk of material. This observation is consistent with the experimental observation of the low heat damage of the remaining of the sample [2]. At 400 ps, in the pure photochemical system the ejection of a big chunk of material is observed. Indeed, this cluster is nearly as dense and as cold as the leftover of the sample. In the combined system, at 400 ps the plume is a network of hot clusters. Void formation or spallation is observed at 40 nm. By 1 ns, all chemical reactions are completed and the samples are cooling off. In the pure photochemical system, the cold dense clusters are separated by low density regions. In the combined system, the clusters are separated by the network of small clusters and monomers, which results in the high density plume.

4. Conclusions

The molecular dynamics simulations of a system containing only photochemical processes show a strong pressure wave propagation and a sharp enthalpy rise, resulting in the ejection of big molecular clusters from the surface. The clusters are colder and denser than clusters in the system where photochemical and thermal processes are present. The top of the plume exhibits high temperatures, whereas the residual part of the sample is cold. The removal of damaged material through big cluster ejection can be attributed to experimental observations of low heat damage of material by far-UV laser irradiation.

Acknowledgements

This work is supported by the Air Force Office of Scientific Research through the Medical Free Electron Laser Program and the Multidisciplinary University Research Initiative, and the Chemistry Division of the National Science Foundation. Computational support was provided by the Center for Academic Computing at Penn State University.

References

[1] A.J. Welch, M. Motamedi, S. Rastegar, G.L. LeCarpentier, D. Jansen, Photochem. Photobiol. 53 (1991) 815.
[2] B.J. Garrison, R. Srinivasan, J. Appl. Phys. 57 (1985) 2909.
[3] T. Ichimura, Y. Mori, H. Shinohara, N. Nishi, Chem. Phys. 189 (1994) 117.
[4] T. Ichimura, Y. Mori, J. Chem. Phys. 58 (1972) 288.
[5] B. Luk'yanchuk, N. Bityurin, S. Anisimov, D. Bäuerle, Appl. Phys. A 57 (1993) 367.
[6] K. Hatanaka, M. Kawao, Y. Tsuboi, H. Fukumura, J. Appl. Phys. 82 (1997) 5799.
[7] Y. Tsuboi, K. Hatanaka, H. Fukumura, H. Masuhara, J. Phys. Chem. 98 (1994) 11237.
[8] Y. Tsuboi, H. Fukumura, H. Masuhara, J. Phys. Chem. 99 (1995) 10305.
[9] R. Srinivasan, B. Braren, Chem. Rev. 89 (1989) 1303.
[10] T. Lippert, C. David, J.T. Dickinson, M. Hauer, U. Kogelschatz, S.C. Langford, O. Nuyken, C. Phipps, J. Robert, A. Wokaun, J. Photochem. Photobiol. A: Chem. 145 (2001) 145.
[11] J. Wei, N. Hoogen, T. Lippert, O. Nuyken, A. Wokaun, J. Phys. Chem. B 105 (2001) 1267.
[12] L.V. Zhigilei, B.J. Garrison, J. Appl. Phys. 88 (2000) 1281.
[13] L.V. Zhigilei, P.B.S. Kodali, B.J. Garrison, J. Phys. Chem. B 101 (1997) 2028, 102 (1998) 2845.
[14] L.V. Zhigilei, P.B.S. Kodali, B.J. Garrison, Chem. Phys. Lett. 276 (1997) 269.
[15] L.V. Zhigilei, B.J. Garrison, Appl. Phys. Lett. 74 (1999) 1341.
[16] L.V. Zhigilei, Y.G. Yingling, T.E. Itina, T.A. Schoolcraft, B.J. Garrison, Int. J. Mass Spectrom., Ion Processes, Franz Hillenkamp, special issue, in press.
[17] Y.G. Yingling, L.V. Zhigilei, B.J. Garrison, J. Photochem. Photobiol. A 145 (2001) 173.
[18] Y.G. Yingling, L.V. Zhigilei, B.J. Garrison, Nucl. Instr. and Meth. B 180 (2001) 171.
[19] Y.G. Yingling, L.V. Zhigilei, B.J. Garrison, A. Koubenakis, J. Labrakis, S. Georgiou, Appl. Phys. Lett. 78 (2001) 1631.

[20] Y.G. Yingling, B.J. Garrison, Chem. Phys. Lett. 364 (2002) 237.
[21] S. Georgiou, A. Koubenakis, M. Syrrou, P. Kontoleta, Chem. Phys. Lett. 270 (1997) 491;
S. Georgiou, A. Koubenakis, J. Labrakis, M. Lassithiotaki, J. Chem. Phys. 109 (1998) 8591;
S. Georgiou, A. Koubenakis, J. Labrakis, M. Lassithiotaki, Appl. Surf. Sci. 127 (1998) 122.
[22] L.V. Zhigilei, B.J. Garrison, Mater. Res. Soc. Symp. Proc. 538 (1999) 491.
[23] E. Dekel, S. Eliezer, Z. Henis, E. Moshe, A. Ludmirsky, I.B. Goldberg, J. Appl. Phys. 84 (1998) 4851.